

Supplementary data

Computational design for injection continuous liquid interface production

Gabriel Lipkowitz¹, Navneeth Krishna¹, Ian Coates², Eric Shaqfeh^{1,2,*}, Joseph DeSimone^{2,3,*}

¹ Department of Mechanical Engineering, Stanford University, Stanford, CA 94305, USA

² Department of Chemical Engineering, Stanford University, Stanford, CA 94305, USA

³ Department of Radiology, Stanford University, Stanford, CA 94305, USA

* Correspondence authors; E-mails: esgs@stanford.edu; jmdesimone@stanford.edu.

Computational modeling of iCLIP 3D printing

A geometric description of our system is illustrated in Supplementary Figure 1. When $\epsilon \ll 1$, the simplified governing lubrication equations for momentum are:

$$\frac{\partial \tilde{p}}{\partial \tilde{z}} \approx 0 \quad (19)$$

$$\tilde{\nabla} \tilde{p} \approx \frac{\partial^2 \tilde{\mathbf{u}}}{\partial \tilde{z}^2} \quad (20)$$

And from continuity:

$$\tilde{\nabla} \cdot \tilde{\mathbf{u}} + \frac{\partial \tilde{u}_z}{\partial \tilde{z}} = 0 \quad (21)$$

with the boundary conditions imposed at the part contour $\tilde{p} = 0$ at $(x, y) \in \Omega(z)$, $\tilde{u}_z(\tilde{z} = 0) = 0$ and $\tilde{u}_z(\tilde{z} = 1) = 1$. Integrating Equation (20) gives the dimensionless fluid velocity in the x and y directions as $\tilde{\mathbf{u}} \approx -\frac{1}{2} \tilde{\nabla} \tilde{p} \tilde{z} (1 - \tilde{z})$ and integrating Equation (21) gives the dimensionless fluid velocity in z direction as $\tilde{u}_z = -\int_0^{\tilde{z}} \tilde{\nabla} \cdot \tilde{\mathbf{u}} dz$. The resulting suction force on object P results from the negative pressure required to support the flow as the build platform moves:

$$\tilde{\nabla}^2 \tilde{p} = 12 \tilde{u}_z(\tilde{z} = 1) \quad (22)$$

Integrated over the footprint of the part gives us an approximation of the force required to offset the suction forces. For a cylindrical part of radius R and $\tilde{u}_z(\tilde{z} = 1)$:

$$F_s = -\frac{3\pi\mu UR^4}{h^3} \quad (23)$$



Copyright©2024 by the authors. Published by ELSP. This work is licensed under Creative Commons Attribution 4.0 International License, which permits unrestricted use, distribution, and reproduction in any medium provided the original work is properly cited.

Materials and methods

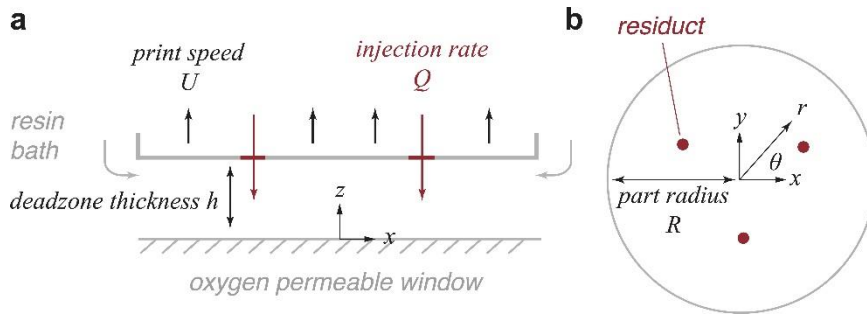


Figure S1. Geometric description of CLIP deadzone modeled in this work, with print speed U , deadzone height h , and part radius R , where $R \gg h$ to justify the lubrication approximation.

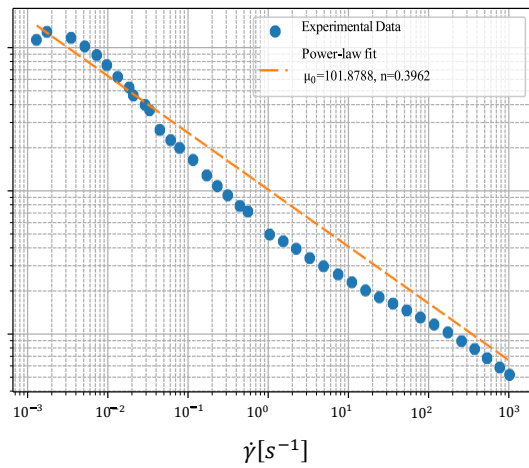


Figure S2. Apparent viscosity of EPU 40 resin fit to the power-law model from Equation 3.

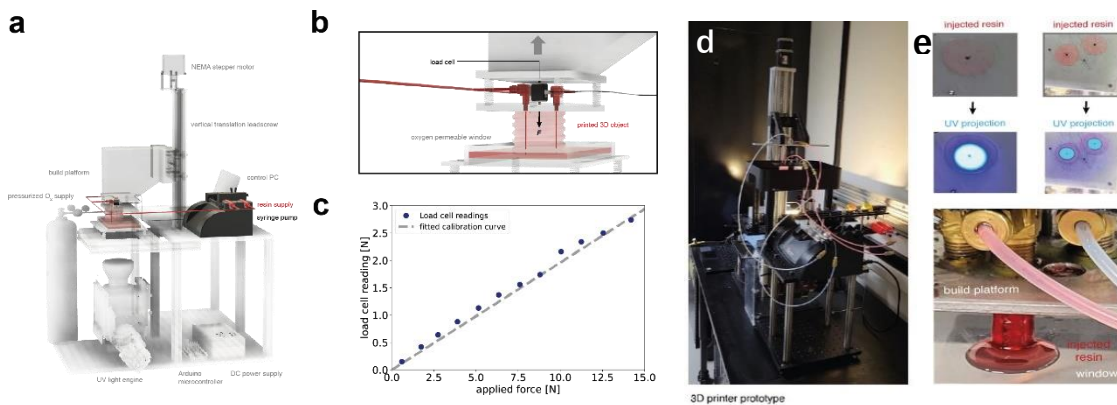


Figure S3. Summary of hardware modifications to state-of-the-art resin 3D printer for injection 3D printing. (a) schematic of iCLIP printer set-up; (b) mechanism by which load cell records Stefan forces; (c) observed linearity in load cell readings; (d) real-world printer set-up; (e) images taken under the vat during printing with injection.

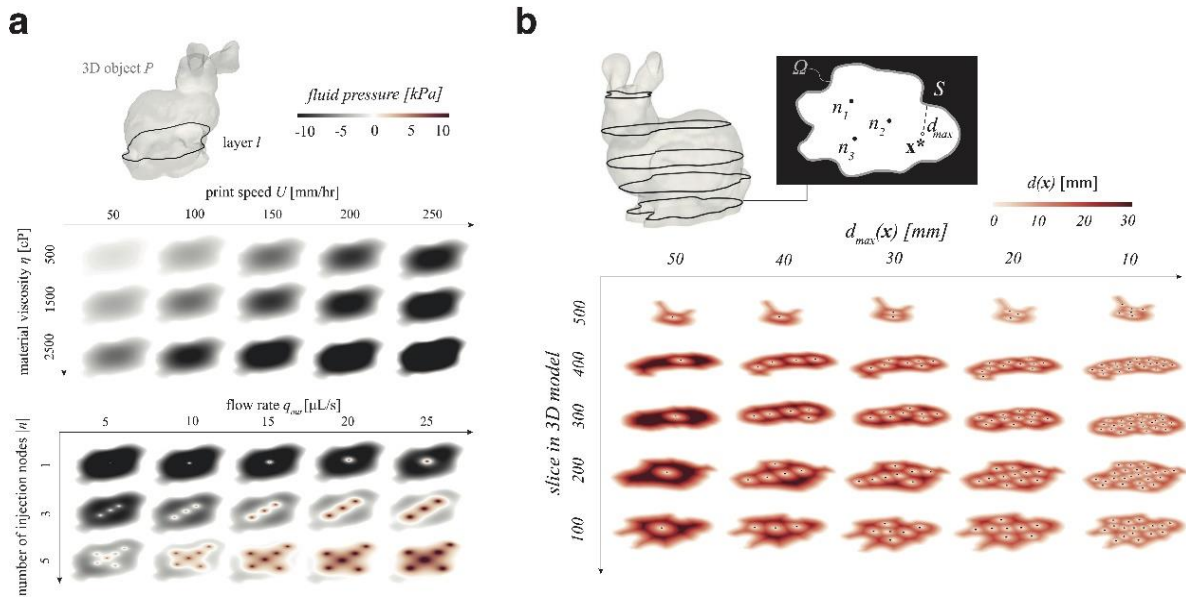


Figure S4. (a) When a given layer l while printing a 3D object P is considered independently, physical parameters such as print speed U and material viscosity η are positive correlated with failure-inducing suction forces F_s . Injection 3D printing incrementally adding high pressure injection sources n , each with a flow rate q_{out} , can offset such suction. (b) Optimization objective for pressure control during vat 3D printing. Our pipeline minimizes the distance d from any pixel representing a point in the printed object to an input fluid source.

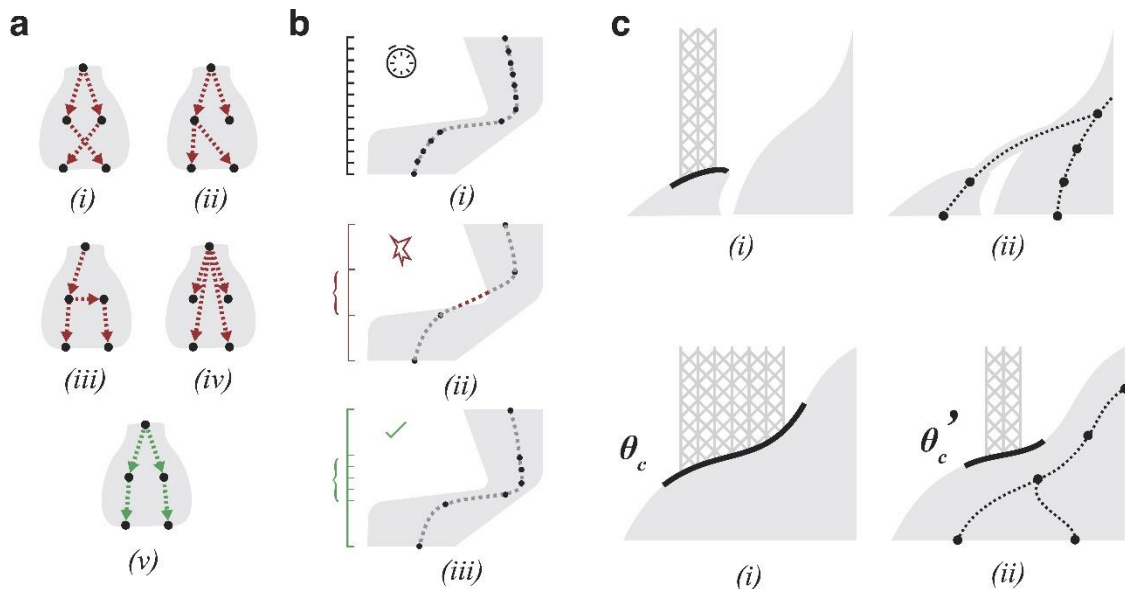


Figure S5. Design tool integration. (a) Hard constraints on the design space. (b) Adaptive slicing approach. (c) Method for integration of our fluidic approach with support structure generators.

Algorithm 1: DIFFERENTIAL EVOLUTION FOR OPTIMIZING POINT POSITIONS

```

1 Function Optimize Point Positions( $C, C_1, C_2$ ):   ▶ Irregular contour  $C$ , Initial points  $C_1, C_2$ 
2 Define objective function  $f$ : Cumulative distance of all positions in  $C$  to nearest point or contour
3 Initialize population with  $C_1, C_2$  and random perturbations                               ▶ DE population
4 while not converged do
5   For each individual in the population:
6   begin
7     Mutate individual using DE strategy                                               ▶ Generate trial vector
8     Crossover with another individual to produce offspring
9     Evaluate offspring using  $f$ 
10    If offspring is better, replace individual                                       ▶ Selection step
11  end
12  Store best individual and its objective function value
13  Check convergence criteria
14 end
15 Extract best positions from the best individual
16 return Optimal positions
  
```

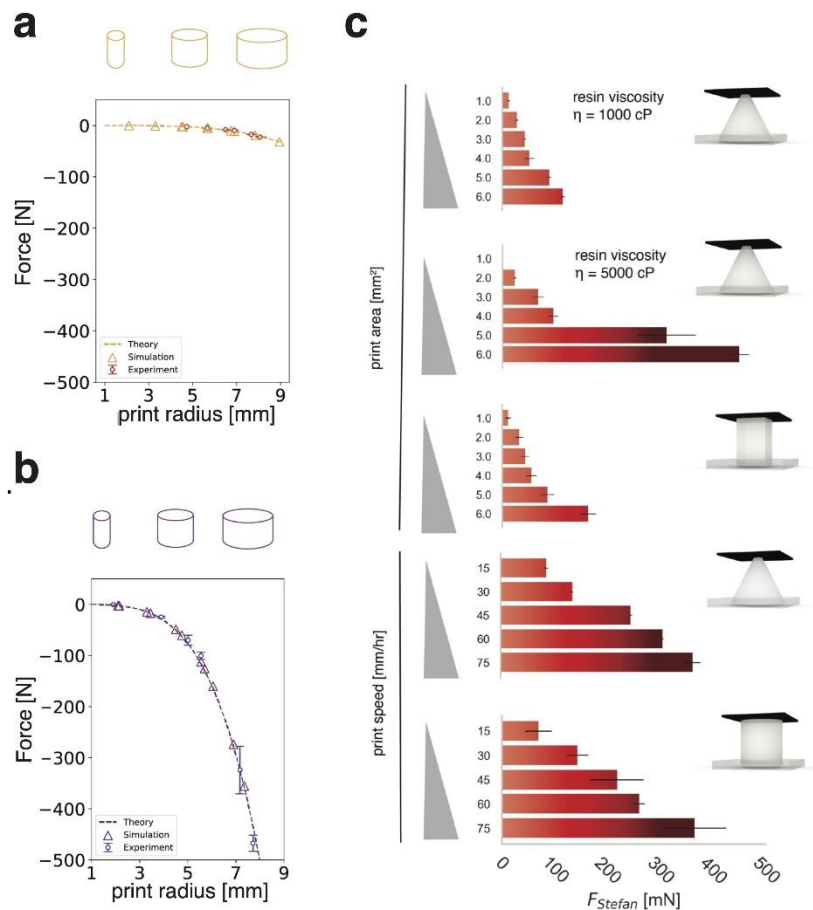


Figure S6. Force reading without injection dependence on geometry and material rheology. Measured Stefan forces while printing geometries with circular cross section (a). For cone of varying radius within a single print, and for cylinder of varying radius between prints with resin of viscosity 500 cP (a) and 1800 cP (b). (c) Multiparameter sweep experiments quantifying the impact of (i) part cross sectional area, (ii) resin viscosity, and (iii) print speed on Stefan force.

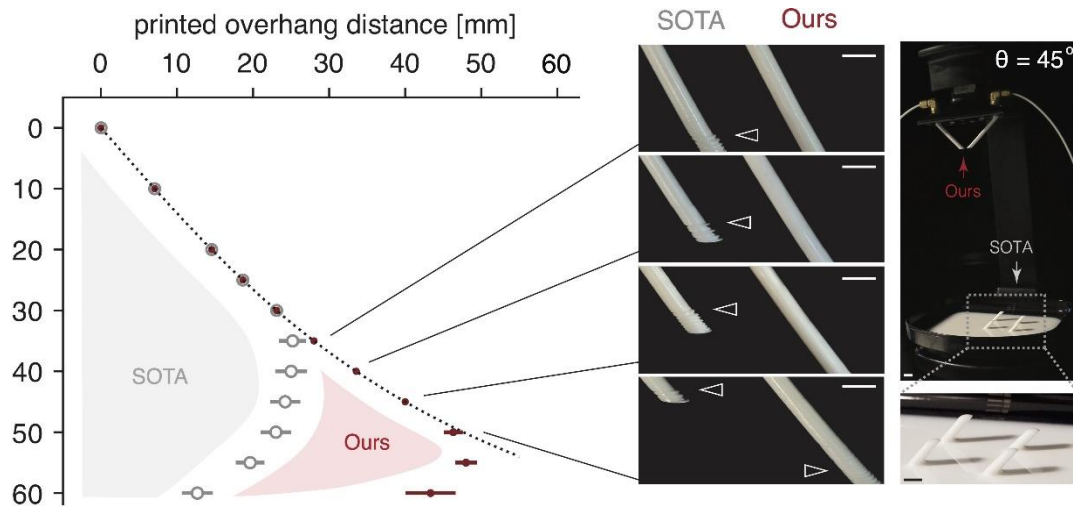


Figure S7. Experimental validation of our approach with primitive geometries. Print results for varying overhang angles by SOTA and our approach for rod geometries. Error bars denoting +/- one standard deviation from mean of technical triplicates. White arrows denote suction-related defects. Scale bars indicate 5 mm.

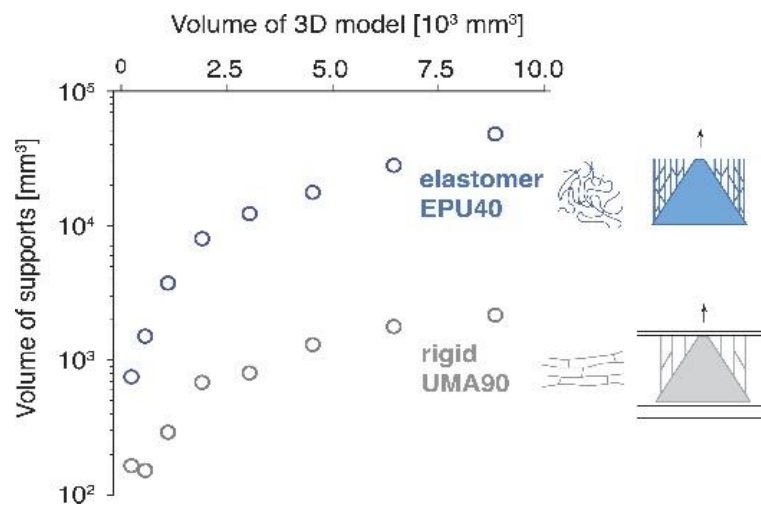


Figure S8. Using a commercial slicer from Carbon 3D, volume of supports required as a function of cone model volume for both rigid (UMA90) and elastomeric (EPU40) resins considered in this work.

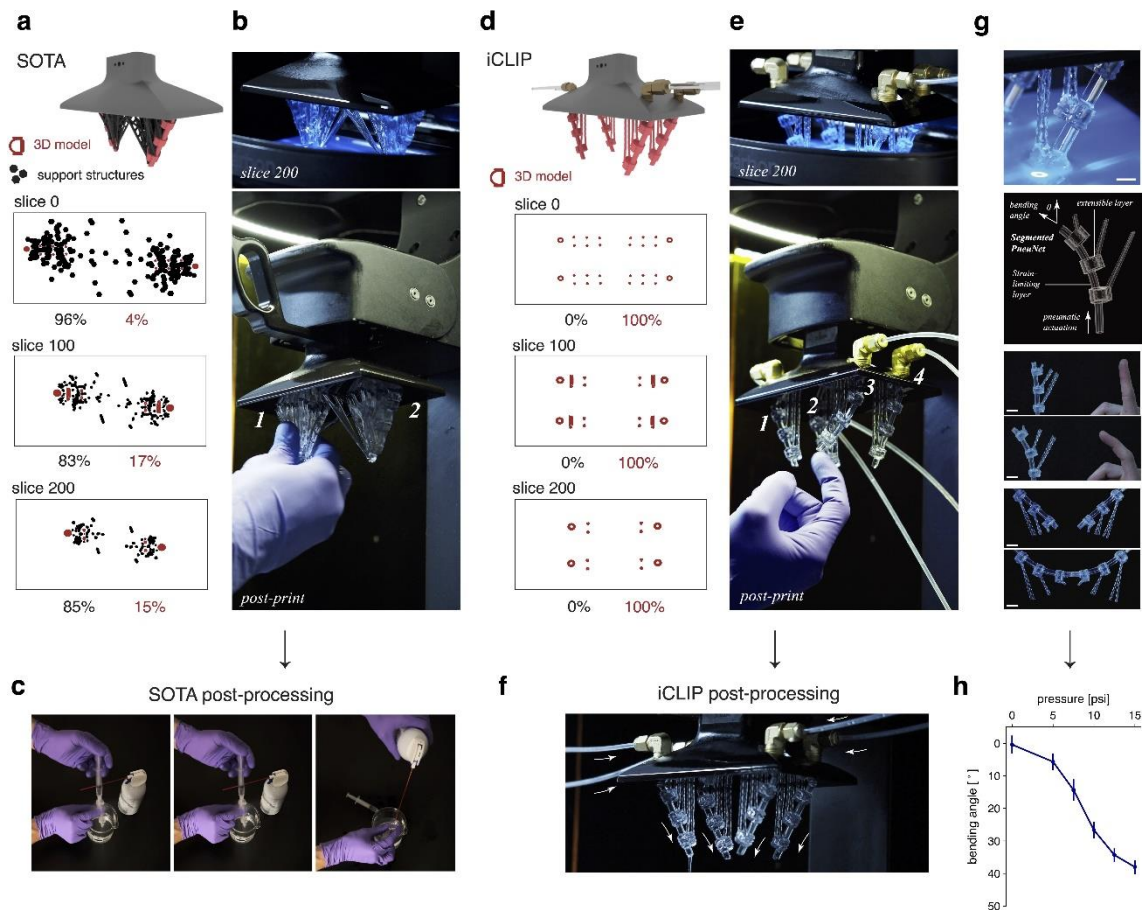


Figure S9. Soft robotics application of iCLIP printing. (a) By state-of-the-art printing, an example bending actuator requires support structures indicated in black, with model itself in red, which provides structural stiffness to the object during printing (b). (c) After printing, as for cleaving supports, cleaning procedures are highly manual. (d)-(e) During iCLIP printing, no supports are needed, liberating space on the platform for more parts. (f) After printing, such channels can be readily cleaned by the same fluidic system used for injection during printing. (g)-(h) For the PneuNet printed by our method, fluid pressure exerted through embedded channels is positively correlated with the bending angle of the soft actuator.